ELECTROCHEMISTRY

CO_2 electroreduction to ethylene via hydroxide-mediated copper catalysis at an abrupt interface

Cao-Thang Dinh,[1]* Thomas Burdyny,[2]* Md Golam Kibria,[1]* Ali Seifitokaldani,[1]* Christine M. Gabardo,[2] F. Pelayo García de Arquer,[1] Amirreza Kiani,[1] Jonathan P. Edwards,[2] Phil De Luna,[3] Oleksandr S. Bushuyev,[1] Chengqin Zou,[1,4] Rafael Quintero-Bermudez,[1] Yuanjie Pang,[2] David Sinton,[2] Edward H. Sargent[1]†

Carbon dioxide (CO_2) electroreduction could provide a useful source of ethylene, but low conversion efficiency, low production rates, and low catalyst stability limit current systems. Here we report that a copper electrocatalyst at an abrupt reaction interface in an alkaline electrolyte reduces CO_2 to ethylene with 70% faradaic efficiency at a potential of −0.55 volts versus a reversible hydrogen electrode (RHE). Hydroxide ions on or near the copper surface lower the CO_2 reduction and carbon monoxide (CO)–CO coupling activation energy barriers; as a result, onset of ethylene evolution at −0.165 volts versus an RHE in 10 molar potassium hydroxide occurs almost simultaneously with CO production. Operational stability was enhanced via the introduction of a polymer-based gas diffusion layer that sandwiches the reaction interface between separate hydrophobic and conductive supports, providing constant ethylene selectivity for an initial 150 operating hours.

The efficient electrochemical conversion of carbon dioxide (CO_2) into valuable carbon-based fuels and feedstocks enables the urgently needed storage of intermittent renewable electricity and, ultimately, a net reduction of greenhouse gas emissions (*1*–*5*). Much effort has been devoted to advance the prospects of producing ethylene, a chemical feedstock in high demand, from CO_2 electroreduction (*6*–*13*). The CO_2 reduction reaction (CO_2-RR) has reached lower activation overpotentials and increased faradaic efficiencies via tuning of catalyst morphologies (*4*, *5*, *10*, *14*, *15*), manipulation of oxidation states (*3*, *16*, *17*), and introduction of dopants (*2*, *18*–*20*). For CO_2 conversion to ethylene, Cu oxide catalysts have achieved peak faradaic efficiencies of 60% by suppressing competing reactions and operating in a narrow reaction window (*13*, *21*–*23*). Separately, ethylene currents of 150 mA cm^{-2} have been achieved at selectivities of 36% and potentials of −0.58 V versus a reversible hydrogen electrode (RHE) on Cu nanoparticles in a flow cell configuration with alkaline electrolytes (*12*).

Despite advances in individual metrics (table S1), large negative potentials are required to reach substantial ethylene selectivities, in part because of the 200- to 300-mV overpotential gap between the formation of necessary CO intermediates and that of ethylene (*24*). Additionally, selective ethylene production has not yet been sustained at commercially relevant current densities (>100 mA cm^{-2}). Stable and highly selective ethylene production at lower overpotentials is urgently needed to enable the renewable electricity–powered synthesis of fuels and feedstocks.

We first pursued experimental and theoretical insights into the direct influence of hydroxide (OH^-) ions, as distinct from bulk pH effects alone, on CO_2 reduction at a Cu catalyst surface. In CO_2 reduction applications, metal oxides have been proposed as active sites even when present in residual or subsurface forms (*16*, *25*, *26*). Hydroxide ions adsorbed or proximate to metal catalysts may play a similar role in modulating active catalytic sites. Further, the reaction rate of the competing hydrogen evolution reaction is suppressed in alkaline electrolytes because of slow kinetics of the first water reduction step (the Volmer step), lowering adsorbed hydrogen surface coverage and influencing the subsequent Heyrovsky and Tafel steps (*27*–*30*).

The direct molecular effects of hydroxide on CO_2 reduction have yet to be studied in detail, in part because canonical H-shaped electrochemical architectures (H cells) are limited by the low availability of CO_2 at pH >10 in aqueous electrolytes. CO_2 dissolved in an alkaline electrolyte will rapidly react, forming a neutral-pH carbonate mixture. Although high-pH conditions can be locally generated in H cells via rapid proton consumption [first from proton reduction, then from water reduction (*31*)], this operation provides information about production at high currents and does not directly elucidate CO_2 reduction onset potentials.

In contrast, a gas diffusion layer positioned immediately adjacent to the catalyst layer allows for CO_2 to diffuse a short distance to the catalyst surface and react before it is converted to bicarbonate. Thus, it is possible for CO_2 reduction to occur under alkaline conditions. We took the view that a flow cell in which the catalyst is deposited onto a gas diffusion layer has the potential to substantially increase the local concentration of gaseous CO_2 and enable clarification of the influence of hydroxides in CO_2-RRs.

We deposited a 100-nm-thick Cu catalyst onto a carbon-based gas diffusion layer (fig. S1), allowing CO_2 reduction under extremely alkaline conditions with the benefit of diffusion of CO_2 across the gas-liquid interface (Fig. 1A). In an Ar environment, the onset potential for H_2 remained relatively constant in the KOH concentration range of 1 to 10 M (Fig. 1B). In a CO_2 environment, the onset potential for the CO_2-RR shifted markedly to more positive potentials with increasing KOH concentrations (Fig. 1B). A similar experiment on a hydrogen-evolving catalyst showed only a minor anodic shift when Ar was replaced by CO_2 (fig. S2), agreeing well with the applied Nernst shift as predicted by a reaction-diffusion model (fig. S3). In 10 M KOH, formation of CO was then observed at a potential 140 mV lower, close to the thermodynamic potential of −0.11 V versus an RHE (Fig. 1C), and the reaction reached >50% selectivity at −0.18 V. Notably, ethylene formation in 10 M KOH occurred at similar potentials: We detected ethylene at applied potentials as low as −0.165 V versus an RHE, only 0.245 V higher than the thermodynamic CO_2-to-ethylene electroreduction potential. This observation is in contrast to our findings with 1 M KOH and prior reports in which the onset potentials of CO and C_2H_4 formation were separated by 200 to 300 mV (*12*, *24*), with one reported ethylene onset occurring at −0.34 V versus an RHE (*9*).

Tafel analyses (Fig. 1E) of ethylene production from CO_2 on the Cu catalyst gave slopes of 135 and 65 mV decade $(dec)^{-1}$ in 1 and 10 M KOH, respectively. Similar slopes for ethylene were also observed in CO reduction on the Cu catalyst (fig. S4), suggesting that the increased hydroxide concentration changes the overall rate-determining step. In contrast to the case of the CO_2-RR, however, the ethylene onset potential when ethylene is produced directly from CO does not shift to lower potentials, implying a further and distinct effect of hydroxide on reaction kinetics.

In the CO_2-RR the onset potential gap between CO and C_2H_4 is attributed to the need to build up coverage of surface-adsorbed CO (*CO) across the catalyst surface before CO dimerization becomes energetically favorable. As the electrolyte pH is increased, the penetration distance of CO_2 into the electrolyte is notably diminished through direct interaction with hydroxide molecules—a point revealed from a reaction-diffusion model analysis (Fig. 1D) analogous to studies presented in prior reports (*32*). In 10 M KOH, the CO_2 present in the electrolyte

[1]Department of Electrical and Computer Engineering, University of Toronto, 10 King's College Road, Toronto, ON M5S 3G4, Canada. [2]Department of Mechanical and Industrial Engineering, University of Toronto, 5 King's College Road, Toronto, ON M5S 3G8, Canada. [3]Department of Materials Science Engineering, University of Toronto, 184 College Street, Toronto, ON M5S 3E4, Canada. [4]Institute of New-Energy Materials, School of Materials Science and Engineering, Tianjin University, Tianjin 300072, China.
*These authors contributed equally to this work.
†Corresponding author. Email: ted.sargent@utoronto.ca

resides mainly within the first 120 nm of the catalyst layer. This arrangement requires CO_2 reduction to take place near an abrupt reaction interface, in contrast with the more distributed reaction interface feasible in 1 M KOH. With little competition from H_2 at these potentials (Fig. 1B), the more localized, and hence concentrated, CO_2 reaction intensity boosts *CO coverage even at modestly negative potentials. This effect improves the reaction kinetics for CO dimerization. This hydroxide-mediated abrupt reaction interface then kinetically allows CO and C_2H_4 to form at similarly low potentials (Fig. 1C). The observed 300-mV shift in ethylene formation from 1 to 10 M KOH is also larger than the pH-dependent shift (59.1 mV/pH unit) observed both experimentally and theoretically for CO reduction to ethylene, where the initial CO_2-to-CO step is avoided (*33*–*36*).

We characterized the catalyst during and after CO_2-RRs in different electrolytes. We used scanning electron microscopy (SEM), transmission electron microscopy (TEM), and in situ x-ray absorption spectroscopy (XAS). In situ XAS of 100-nm samples (fig. S5) showed that at the open-circuit potential, Cu becomes oxidized when submerged in 5 M KOH, most likely via formation of surface hydroxides. However, when a negative potential of −0.16 or −0.96 V versus an RHE is applied, the observed spectra closely match those of fully-reduced pristine Cu foil (fig. S5). We conclude that, under the applied reducing potential used during the CO_2-RR, the surface is primarily Cu^0 and remains consistent over the range of potentials and concentrations of interest. The SEM and TEM characterization of the sample after CO_2-RRs in 1, 5, and 10 M KOH electrolyte showed similar Cu morphologies and crystalline structures, from which we argue that structure morphology did not play a predominant role in the enhanced CO_2-RR we observed at high KOH concentrations (figs. S1 and S6).

To supplement these experimental findings, we used density functional theory (DFT) to assess the impact of hydroxide ions on the thermodynamic and activation energy barriers of the CO dimerization step. CO dimerization is the rate-determining step for C_2 products at high pHs and low applied potentials (*22*, *35*). We performed this analysis on Cu(111), (100), and (110) surfaces, including explicit water molecules in the computational studies (figs. S7 to S10 and tables S2 to S11). The DFT results suggest that the presence of hydroxide lowers the binding energy of CO on the Cu surface. On all surfaces, hydroxide is found to also increase the charge imbalance between carbon atoms in adsorbed OCCO, further stabilizing this intermediate through a stronger dipole attraction within OCCO. The combined differences lead to an overall decrease in the activation energy barrier for the CO dimerization step, lowering the energy barrier by 156 meV on Cu(100) with an OH^- surface coverage of two OH^- ions per 16 Cu atoms [a 2/16 monolayer (ML)] (fig. S9).

With the decreased Tafel slope and matching onset potentials of CO and C_2H_4 in 10 M KOH, high ethylene selectivities at low overpotentials become feasible. By increasing the reaction rate over a fixed electrochemically active surface area, we can control the relative kinetics of CO desorption and dimerization to drive ethylene formation. As seen in Fig. 1D, the abrupt reaction interface and the use of high KOH concentrations contribute to achieving this goal by limiting CO_2 penetration to a fraction of the catalyst layer, reducing the specific active area where the CO_2-RR occurs. Therefore, we sought to similarly constrain the electrochemically active surface

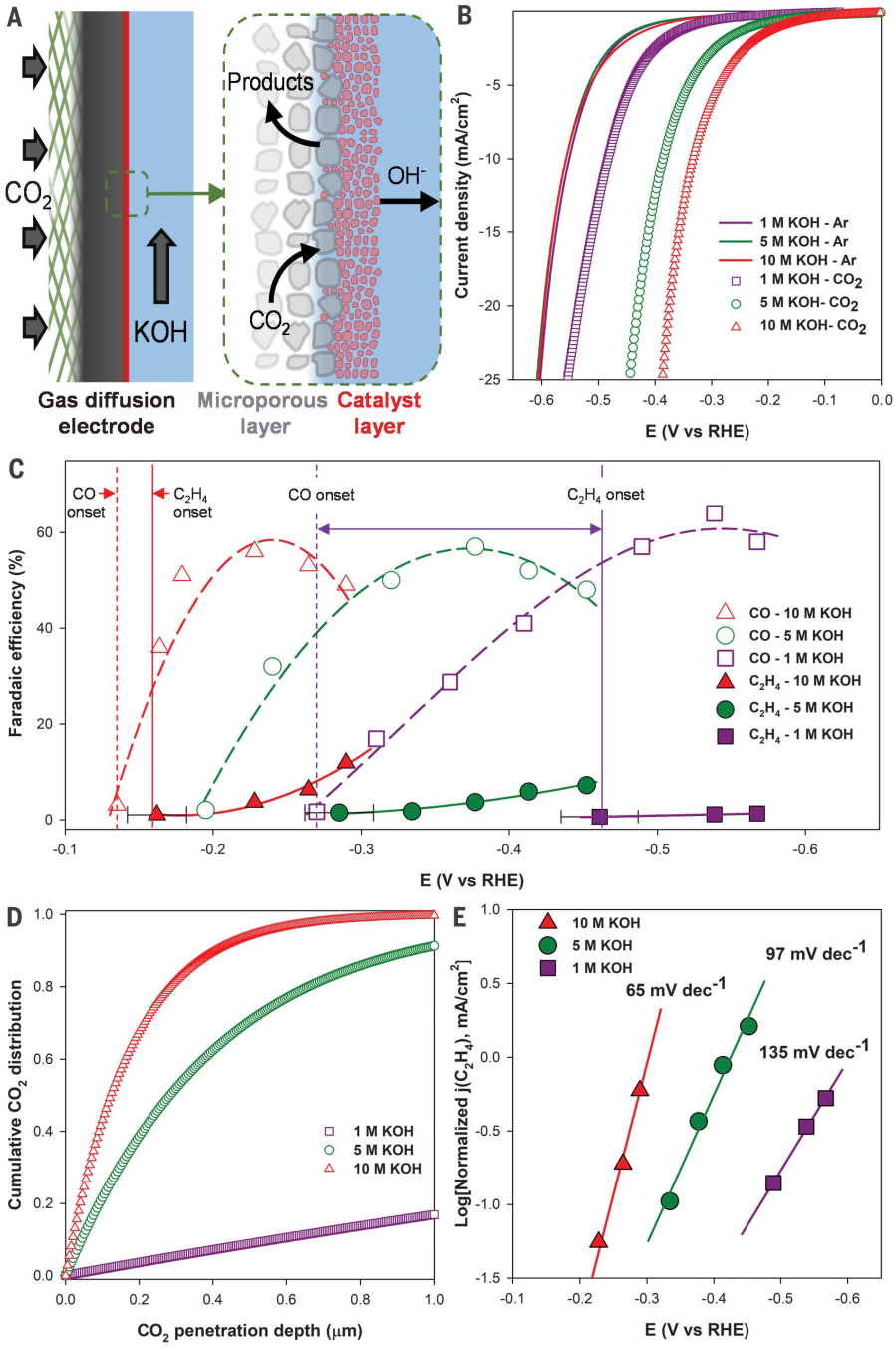

Fig. 1. Experimental studies of the effect of hydroxide on CO_2 reduction, hydrogen evolution, and CO-CO coupling. (**A**) Schematic of the cathode portion of a gas diffusion electrode for CO_2. (**B**) Linear sweep voltammetry scan in various KOH electrolyte concentrations showing low overpotential CO_2 reduction in high KOH concentrations. E, electrode potential. (**C**) C_2H_4 and CO faradaic efficiencies showing the reduction of C_2H_4 onset potential with increasing KOH concentrations. Values are means, and error bars indicate SD (n = 3 replicates). (**D**) Modeling of the cumulative CO_2 distribution across the catalyst layer at 0 mA cm^{-2} and different KOH concentrations. (**E**) Partial ethylene current densities and Tafel slope with increasing KOH concentrations. j, electric current density.

area of the catalyst layer by using thermal evaporation to tune the thickness of the CO_2 reduction interface in the flow cell configuration (Fig. 1A). We used deposition thicknesses of 10 and 25 nm and compared with a thermally deposited thickness of 1000 nm, all deposited on a carbon-based gas diffusion layer. For further comparison, we deposited commercial Cu nanoparticles (particle size, <50 nm) at a loading concentration of 1000 μg/cm^2 by using a drop-casting technique. We characterized nanoparticle size and surface morphology by SEM and scanning TEM for particle sizes ranging from 15 to 40 nm (figs. S11 and S12). Ex situ x-ray photoelectron spectroscopy (XPS) of all three samples showed the presence of C, Cu, and O (fig. S13). The Cu peaks indicated a mixture of metallic Cu and Cu^{2+}. X-ray powder diffraction confirmed the crystalline structure of the samples. The catalyst loadings, analyzed with the use of inductively coupled plasma atomic emission spectrometry (ICP-AES), were ~11, 28, and 1100 μg for the thermally deposited 10-, 25-, and 1000-nm samples, respectively. In CO_2-RR tests in an H cell configuration using 0.1 M $KHCO_3$ electrolyte, these samples exhibited C_2H_4 faradaic efficiency comparable to that of reported Cu and oxide-derived Cu catalysts (fig. S14 and table S13).

The CO_2-RR activities of the Cu samples were evaluated in the flow cell reactor with 10 M KOH (Fig. 2A and figs. S15 to S17). At less-negative potentials (−0.4 V versus an RHE and potentials closer to zero), the samples showed similar slopes, indicative of similar levels of intrinsic activity. The two thicker samples showed higher current densities than the 10- and 25-nm samples at similar potentials, indicating that the higher catalyst loading distributes the reaction beyond 25 nm, as predicted in Fig. 1D. At more-negative potentials, however, the reaction rates on the thinner samples were higher than those on the thicker samples, resulting in similar current densities at −0.54 V versus an RHE. When we analyzed product selectivities in 10 M KOH, we found that the samples showed optimal ethylene production in the current range of 225 to 275 mA cm^{-2} (Fig. 2B), as CO selectivity decreased with current density (fig. S16). Both the 10- and 25-nm samples showed an ethylene faradaic efficiency higher than 60%, with the 25-nm sample peaking at 66% ethylene and exhibiting ethanol at 11% and acetate at 6% (figs. S16 and S17). Overall, the 25-nm sample showed a total C_2 selectivity of 83% at 275 mA cm^{-2} and a low potential of −0.54 V versus an RHE, corresponding to a half-cell ethylene conversion efficiency of 44% (table S1). The 25-nm narrow reaction interface also enabled a high ethylene mass activity of 6.5 A mg^{-1} (table S1 and fig. S16).

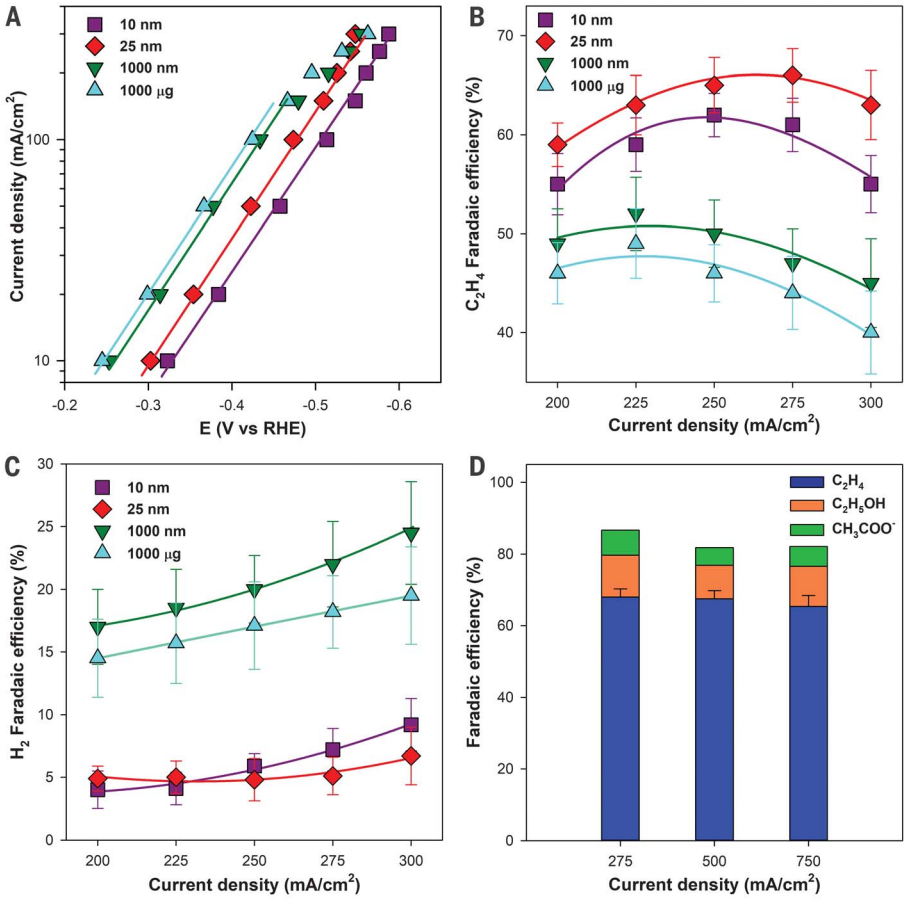

Fig. 2. Hydroxide-mediated CO_2 reduction performance on abrupt reaction interface catalysts. (**A**) Geometric reduction current density as a function of applied potential with 10 M KOH electrolyte on Cu samples of varying thickness. The 10-, 25-, and 1000-nm samples were thermally deposited, and the 1000-μg sample used drop-casted nanoparticles. (**B**) C_2H_4 faradaic efficiencies in the current density range of 200 to 300 mA cm^{-2}, showing the increased C_2H_4 selectivity of the abrupt reaction interface samples (10 and 25 nm) compared with that of thicker samples (1000 nm and 1000 μg) that allow for a more distributed reaction. (**C**) H_2 faradaic efficiencies showing lower H_2 generation on abrupt interface catalysts. (**D**) Optimization of electrolyte for high C_2H_4 selectivity on a 25-nm sample: 10 M KOH (at 275 mA cm^{-2}), 5.5 M KOH with 4 M KI (at 500 mA cm^{-2}), and 3.5 M KOH with 5 M KI (at 750 mA cm^{-2}). Values are means, and error bars indicate SD (n = 3 replicates).

The higher CO_2 reduction selectivities achieved on the thinner catalyst layers were attributable in part to a decrease in H_2 production as a proportion of the total current density, from >15% in the case of the 1000-nm sample to only 5% (Fig. 2C). As shown in Fig. 1B, with the aid of a large CO_2 supply and a low applied potential, CO_2 reduction is favored over H_2 evolution. At higher currents and potentials, the CO_2-RR can also suppress H_2 evolution by occupying surface sites. In highly alkaline conditions, however, a portion of the 1000-nm catalyst layer is largely devoid of CO_2 (Fig. 1D and fig. S3), leaving H_2 evolution as the only possible reaction pathway in this region at higher potentials. These results indicate the need to limit the thickness of the catalyst layer at higher current densities and potentials to prevent unwanted H_2 evolution. The effect of reduced CO_2 availability on CO_2-RR selectivity could also be observed at non–CO_2-limited current densities in 1 M KOH on the 25-nm sample by lowering the partial pressure of CO_2 in the gas phase (fig. S18).

Although the most efficient ethylene production occurred in 10 M KOH, similar ethylene selectivities were achieved at higher partial current densities with a thinner catalyst layer and lower KOH concentrations. By using a thin catalyst to create a catalyst-mediated abrupt reaction interface for the CO_2-RR, we could partially replicate the effect of using 10 M KOH to create a hydroxide-mediated abrupt reaction interface (Fig. 1D). Using a catalyst thickness of 25 nm, we achieved ethylene selectivities of 66, 65, and 63% at total current densities of 275, 500, and 750 mA cm^{-2} in KOH concentrations of 10, 5.5, and 3.5 M, respectively; in each case KI was added to replace the missing potassium (Fig. 2D). KI was chosen because iodide in the electrolyte is known to increase CO_2 reduction activity by accelerating the hydrogenation of the key adsorbed CO intermediate (*37*). We then achieved an ethylene partial current density of

473 mA cm^{-2} at only −0.67 V versus an RHE (fig. S19).

Although high electrochemical performance is achieved with the traditional carbon-based gas diffusion layer architecture, the stability of catalysts on these substrates was poor. The carbon-based gas diffusion electrode degrades (fig. S20) within 1 hour of continuous CO_2-RR operation, regardless of catalyst thickness (25 and 1000 nm) or electrolyte concentration (1 and 7 M KOH). We studied the stability of the carbon-based gas diffusion electrode itself by carrying out electroreduction on a gas diffusion layer without a Cu catalyst. The results show that the oxygen content in the gas diffusion layer doubled and that the surface of carbon turned from hydrophobic to hydrophilic when a negative potential of −0.4 to −0.8 V versus an RHE was applied (fig. S21). We concluded that the instability of the Cu on a carbon-based gas diffusion electrode arose because the gas diffusion layer became flooded as its hydrophobicity was lost during operation. Once the gas diffusion layer floods, the pathways for the diffusion of CO_2 in the gas phase toward the catalyst become obstructed and high CO_2 reduction currents can no longer be sustained.

To improve stability, we sought to develop a new electrode configuration that decoupled the hydrophobic and current collection requirements of traditional carbon-based gas diffusion layers (Fig. 1A). Instead of relying on a single multifunctional layer, we separated the polytetrafluoroethylene (PTFE) and carbon nanoparticles (NPs) into two layers that sandwich our Cu catalyst while maintaining an abrupt reaction interface (Fig. 3A). In this configuration (graphite/carbon NPs/Cu/PTFE electrode) the pure PTFE layer acts as a more stable hydrophobic gas diffusion layer that prevents flooding, and the presence of carbon NPs and graphite stabilizes the Cu catalyst surface. To fabricate the new polymer-based gas diffusion electrode, we sputtered a Cu catalyst layer onto a porous PTFE membrane with a pore size of 220 nm (Fig. 3C). Carbon black nanoparticles were then spray-coated on top to electrically connect the catalyst layer and provide a uniform distribution of current density over the geometric surface (fig. S22). An added graphite layer acted as an overall support and current collector. The thin Cu layer is seen sandwiched between the two layers in a cross-sectional SEM image showing that the abrupt CO_2 reaction interface is conserved in this configuration (Fig. 3B). XPS characterization (fig. S22) revealed that the sample consisted mainly of Cu^0 and Cu^{2+}.

The new electrode showed high CO_2-RR selectivity relative to H_2 evolution in 7 M KOH, similar to the carbon-based gas diffusion electrode (table S13). Although the addition of the carbon NPs between Cu and graphite did not affect the total current density (fig. S23), the ethylene faradaic efficiency rose to 70% (Fig. 3D). The additional carbon support may contribute to a more even distribution of current across the Cu electrode while inhibiting the diffusion of OH^- to the bulk electrolyte, further diminishing CO production to 3% (fig. S23). To evaluate the possibility that carbon NPs could act as a carbon source, we performed the CO_2-RR with isotopic $^{13}CO_2$ as the feedstock. The data show that all of the produced ethylene was derived from $^{13}CO_2$ (fig. S24).

The new graphite/carbon NPs/Cu/PTFE electrode operated for 150 hours without a loss in ethylene selectivity at current densities between

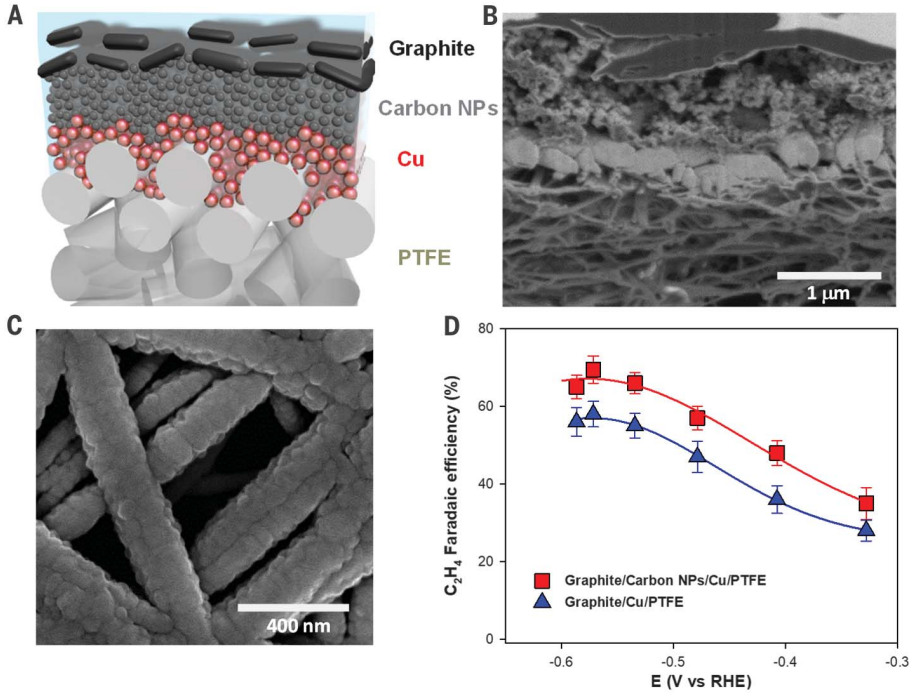

Fig. 3. Structure and performance of the polymer-based gas diffusion electrode. (**A**) Schematic illustration of the graphite/carbon NPs/Cu/PTFE electrode. (**B**) Cross-sectional SEM image of a fabricated graphite/carbon NPs/Cu/PTFE electrode. (**C**) SEM image of Cu nanoparticles sputtered on the PTFE membrane. (**D**) Comparison of ethylene faradaic efficiencies on graphite/carbon NPs/Cu/PTFE and graphite/Cu/PTFE electrodes for CO_2-RR in 7 M KOH electrolyte. Values are means, and error bars indicate SD (n = 3 replicates).

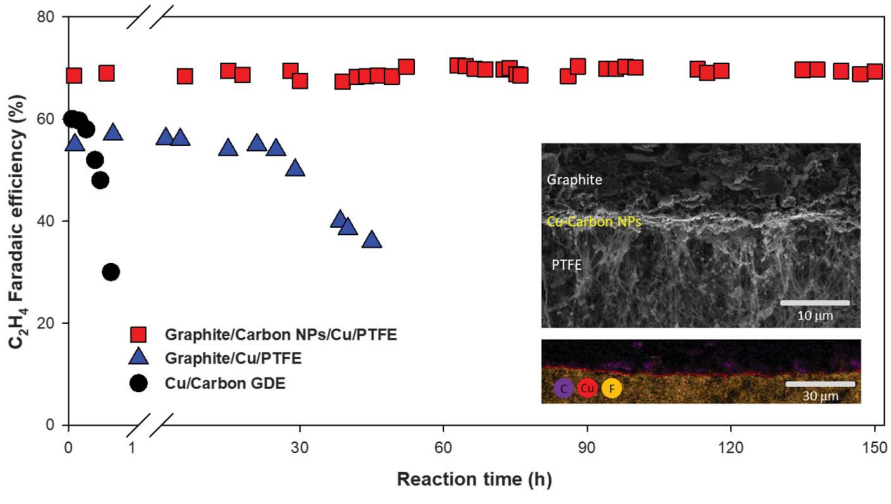

Fig. 4. Stability test of the polymer-based electrode. Long-term performance test of CO_2 reduction to ethylene in 7 M KOH showing high selectivity stability of the graphite/carbon NPs/Cu/PTFE electrode compared with that of a traditional carbon-based gas diffusion electrode (GDE). The stability of a graphite/Cu/PTFE electrode is shown for comparison to highlight the importance of the carbon NPs as a contacting and stabilizing layer. Insets show the cross-section SEM and energy-dispersive x-ray spectroscopy mapping of the sample after 150 hours of continuous CO_2 reduction operation. The stability test was performed at a constant applied voltage of −0.55 V versus the RHE. The current gradually decreased from 100 to 75 mA cm^{-2} over 150 hours of operation.

75 and 100 mA cm^{-2} (Fig. 4 and fig. S25). This performance demonstrates a 300-fold increase in the operating lifetime compared with that of the Cu/carbon gas diffusion layer. The graphite/carbon NPs/Cu/PTFE design also provided longer, higher, and more consistent ethylene selectivities than the same electrode configuration without carbon NPs because of the more mechanically and electrically connected catalyst layer (figs. S25 and S26). Because CO_2 conversion to hydrocarbons is usually carried out at very negative potentials (such as −1 V versus an RHE), material restructuring—even in milder electrolytes and at lower operating currents—can occur over time, and few catalysts have demonstrated sustained high ethylene selectivities over 1 hour of operation (table S13). We propose that the low overpotential required in our system may contribute to avoiding excessive surface reconstruction (*38*) and may be a factor in the observed stable selectivity for ethylene. The observed decrease in current density on the graphite/carbon NPs/Cu/PTFE catalyst over extended operating times is equivalent to a 20-mV increase in potential (fig. S23).

The new electrode configuration shows promise as an easy-to-construct and highly stable system that is compatible with a variety of different catalysts and operating conditions, as demonstrated here by the long-term stability in 7 M KOH. Stable testing in highly alkaline conditions is also important practically, as a high-conductivity electrolyte will likely be required to reduce ohmic losses and boost the overall efficiency of an entire cell. Operating in 10 M KOH versus 0.1 M $KHCO_3$, for instance, results in a decrease in ohmic overpotentials by a factor of 47.

We combined the graphite/carbon NPs/Cu/PTFE cathode with a $NiFeO_x$ (*39*) oxygen evolution catalyst (fig. S27) to perform a full-cell operation in 7 M KOH electrolyte (fig. S28). The system delivers a full-cell energy efficiency for conversion to ethylene of 34% [without the benefit of ohmic resistance (*i*R) correction] at an applied voltage of 2.4 V and an average current density of 110 mA cm^{-2} over 1 hour of operation.

The concept of forming an abrupt reaction interface at a catalyst in highly alkaline media enabled advances in the combination of ethylene electroproduction current density, selectivity, and operating lifetime. The resultant electrical-to-chemical power conversion efficiency, when coupled with the operating stability, indicates a promising platform for CO_2 reduction applications.

REFERENCES AND NOTES

1. M. Schreier *et al.*, *Nat. Energy* **2**, 17087 (2017).
2. S. Lin *et al.*, *Science* **349**, 1208–1213 (2015).
3. S. Gao *et al.*, *Nature* **529**, 68–71 (2016).
4. R. Kas *et al.*, *Nat. Commun.* **7**, 10748 (2016).
5. M. Liu *et al.*, *Nature* **537**, 382–386 (2016).
6. K. D. Yang *et al.*, *Angew. Chem. Int. Ed.* **56**, 796–800 (2017).
7. A. Loiudice *et al.*, *Angew. Chem. Int. Ed.* **55**, 5789–5792 (2016).
8. F. S. Roberts, K. P. Kuhl, A. Nilsson, *Angew. Chem. Int. Ed.* **54**, 5179–5182 (2015).
9. T. T. Hoang, S. Ma, J. I. Gold, P. J. Kenis, A. A. Gewirth, *ACS Catal.* **7**, 3313–3321 (2017).
10. C. Reller *et al.*, *Adv. Energy Mater.* **7**, 1602114 (2017).
11. J. Wu *et al.*, *Nat. Commun.* **7**, 13869 (2016).
12. S. Ma *et al.*, *J. Power Sources* **301**, 219–228 (2016).
13. H. Mistry *et al.*, *Nat. Commun.* **7**, 12123 (2016).
14. Y. Li *et al.*, *Nano Lett.* **17**, 1312–1317 (2017).
15. P. De Luna *et al.*, *Nat. Catal.* **1**, 103–110 (2018).
16. Y. Chen, C. W. Li, M. W. Kanan, *J. Am. Chem. Soc.* **134**, 19969–19972 (2012).
17. D. Ren *et al.*, *ACS Catal.* **5**, 2814–2821 (2015).
18. J. Wu *et al.*, *ACS Nano* **9**, 5364–5371 (2015).
19. D. Kim *et al.*, *J. Am. Chem. Soc.* **139**, 8329–8336 (2017).
20. S. Ma *et al.*, *J. Am. Chem. Soc.* **139**, 47–50 (2017).
21. R. Kas, R. Kortlever, H. Yilmaz, M. T. M. Koper, G. Mul, *ChemElectroChem* **2**, 354–358 (2015).
22. H. Xiao, T. Cheng, W. A. Goddard 3rd, R. Sundararaman, *J. Am. Chem. Soc.* **138**, 483–486 (2016).
23. Y. Lum, B. Yue, P. Lobaccaro, A. T. Bell, J. W. Ager, *J. Phys. Chem. C* **121**, 14191–14203 (2017).
24. Y. Huang, A. D. Handoko, P. Hirunsit, B. S. Yeo, *ACS Catal.* **7**, 1749–1756 (2017).
25. M. Favaro *et al.*, *Proc. Natl. Acad. Sci. U.S.A.* **114**, 6706–6711 (2017).
26. C. Liu *et al.*, *J. Phys. Chem. C* **121**, 25010–25017 (2017).
27. R. Subbaraman *et al.*, *Science* **334**, 1256–1260 (2011).
28. Y. Y. Birdja, M. T. M. Koper, *J. Am. Chem. Soc.* **139**, 2030–2034 (2017).
29. V. R. Stamenkovic, D. Strmcnik, P. P. Lopes, N. M. Markovic, *Nat. Mater.* **16**, 57–69 (2016).
30. W. Sheng, M. Myint, J. G. Chen, Y. Yan, *Energy Environ. Sci.* **6**, 1509–1512 (2013).
31. H. Ooka, M. C. Figueiredo, M. T. M. Koper, *Langmuir* **33**, 9307–9313 (2017).
32. N. Gupta, M. Gattrell, B. MacDougall, *J. Appl. Electrochem.* **36**, 161–172 (2006).
33. K. J. P. Schouten, Z. Qin, E. Pérez Gallent, M. T. M. Koper, *J. Am. Chem. Soc.* **134**, 9864–9867 (2012).
34. J. H. Montoya, C. Shi, K. Chan, J. K. Nørskov, *J. Phys. Chem. Lett.* **6**, 2032–2037 (2015).
35. J. D. Goodpaster, A. T. Bell, M. Head-Gordon, *J. Phys. Chem. Lett.* **7**, 1471–1477 (2016).
36. K. J. P. Schouten, E. Pérez Gallent, M. T. M. Koper, *J. Electroanal. Chem.* **716**, 53–57 (2014).
37. A. S. Varela, W. Ju, T. Reier, P. Strasser, *ACS Catal.* **6**, 2136–2144 (2016).
38. Y.-G. Kim *et al.*, *J. Electroanal. Chem.* **780**, 290–295 (2016).
39. X. Lu, C. Zhao, *Nat. Commun.* **6**, 6616 (2015).

ACKNOWLEDGMENTS

We thank D. Kopilovic and R. Wolowiec for electrochemical cell design and setup and C. S. Tan and A. Proppe for high-resolution TEM and XPS measurements. We thank Y. Hu for XAS support. **Funding:** This work was financially supported by TOTAL American Services, the Connaught Fund, the Ontario Research Fund: Research Excellence Program, the Natural Sciences and Engineering Research Council (NSERC) of Canada, and the CIFAR Bio-Inspired Solar Energy program. All DFT computations were performed on the IBM BlueGene/Q supercomputer with support from the Southern Ontario Smart Computing Innovation Platform (SOSCIP). SOSCIP is funded by the Federal Economic Development Agency of Southern Ontario, the Province of Ontario, IBM Canada, Ontario Centres of Excellence, Mitacs and 15 Ontario academic member institutions. We acknowledge the Toronto Nanofabrication Centre (TNFC) and the Ontario Centre for the Characterization of Advanced Materials (OCCAM) for sample preparation and characterization facilities. X-ray spectroscopy measurements were performed at the Canadian Light Source (SXRMB beamline). A.S. thanks Fonds de Recherche du Quebec–Nature et Technologies (FRQNT) for support in the form of a postdoctoral fellowship award. M.G.K. acknowledges a Banting postdoctoral fellowship from the government of Canada. T.B. thanks Hatch for a graduate scholarship for sustainable energy research. J.P.E. thanks NSERC, Hatch, and the government of Ontario for their support through graduate scholarships. P.D.L thanks NSERC for financial support in the form of the Canada Graduate Scholarship–Doctoral (CGS-D) award. C.M.G. and O.S.B. thank NSERC for financial support in the form of a postdoctoral fellowship. C.Z. acknowledges support from the International Academic Exchange Fund for Joint Ph.D. Students from Tianjin University. **Author contributions:** E.H.S. and D.S. supervised the project. C.-T.D., T.B., M.G.K., and A.S. designed and carried out all of the experiments. A.S. carried out the DFT simulation. T.B. carried out the reaction-diffusion simulation. M.G.K., F.P.G.D.A., and A.K. prepared the evaporated catalysts. P.D.L. and O.S.B. performed the XAS measurements. C.Z. performed the ICP-AES analysis. C.M.G. and Y.P. performed the SEM measurements. R.Q.-B. carried out the XPS analysis. C.-T.D. and J.P.E. designed the electrodes and electrochemical cells. All authors discussed the results and assisted during manuscript preparation. **Competing interests:** C.-T.D., T.B., M.G.K., A.S., D.S., and E.H.S. of the University of Toronto have filed provisional patent application no. 62522925 regarding the preparation of an abrupt catalyst interface for CO_2 reduction. **Data and materials availability:** All data are reported in the main text and supplementary materials.

SUPPLEMENTARY MATERIALS

www.sciencemag.org/content/360/6390/783/suppl/DC1
Materials and Methods
Figs. S1 to S28
Tables S1 to S13
References (*40*–*58*)

3 January 2018; accepted 3 April 2018
10.1126/science.aas9100

Science

CO_2 electroreduction to ethylene via hydroxide-mediated copper catalysis at an abrupt interface

Cao-Thang Dinh, Thomas Burdyny, Md Golam Kibria, Ali Seifitokaldani, Christine M. Gabardo, F. Pelayo García de Arquer, Amirreza Kiani, Jonathan P. Edwards, Phil De Luna, Oleksandr S. Bushuyev, Chengqin Zou, Rafael Quintero-Bermudez, Yuanjie Pang, David Sinton and Edward H. Sargent

Science **360** (6390), 783-787.
DOI: 10.1126/science.aas9100

A very basic pathway from CO_2 to ethylene

Ethylene is an important commodity chemical for plastics. It is considered a tractable target for synthesizing renewable resources from carbon dioxide (CO_2). The challenge is that the performance of the copper electrocatalysts used for this conversion under the required basic reaction conditions suffers from the competing reaction of CO_2 with the base to form bicarbonate. Dinh *et al.* designed an electrode that tolerates the base by optimizing CO_2 diffusion to the catalytic sites (see the Perspective by Ager and Lapkin). This catalyst design delivers 70% efficiency for 150 hours.

Science, this issue p. 783; see also p. 707